ELSEVIER

Earth and Planetary Science Letters 201 (2002) 127–142

EPSL

www.elsevier.com/locate/epsl

Antarctic environmental variability since the late Miocene: ODP Site 745, the East Kerguelen sediment drift

Leah H. Joseph *, David K. Rea, Ben A. van der Pluijm, James D. Gleason

Department of Geological Sciences, University of Michigan, Ann Arbor, MI 48109-1063, USA

Received 25 October 2001; received in revised form 1 April 2002; accepted 10 April 2002

Abstract

Characterization of sediment from Ocean Drilling Program Site 745, representing the East Kerguelen Ridge sediment drift, addresses important issues surrounding the timing of Miocene to present East Antarctic ice sheet stability and oceanic environmental change. Our results show three periods of greatly enhanced accumulation of Antarctic-derived sediment, at 6.4–5.9 Ma, 4.9–4.4 Ma and 1.1–0.8 Ma, potentially indicative of warmer, less stable ice sheets at these times. Conversely, the accumulation of Antarctic-derived material is comparatively less during the middle of the Pliocene warm epoch (4.8–3.2 Ma). The deep flow forming the Kerguelen drift was stronger during the latest Miocene and earliest Pliocene and has decreased in intensity continuously since then.

Keywords: East Antarctica; Antarctic ice sheet; Kerguelen Plateau; sediments; Pliocene; Paleoclimatology; ODP Site 745

1. Introduction

Public concern regarding the effects of global warming often focuses on the effects of rising sea level. Indeed, the melting of just the small, relatively unstable West Antarctic Ice Sheet (WAIS, 3.3×10^6 km^3) would result in a sea level rise of approximately 5 m (Fig. 1). Melting of both the WAIS and the East Antarctic Ice Sheet (EAIS; 26×10^6 km^3) entirely would result in a 70 m sea level rise [1–4].

There have been many investigations into the degree of stability of the East Antarctic Ice Sheet (EAIS) during the Pliocene (e.g. [2,5–13]). Interest in the stability of the EAIS during this period, which encompasses the Pliocene warm interval (4.8–3.2 Ma) [14–16], stems from the need to understand the relationship of Antarctic climate, ice volume, eustatic sea level rise, and Southern Ocean circulation with the global climate system at a time when Earth's conditions might be similar to those achieved through future global warming (e.g. [9]).

Some workers believe that the EAIS reached its present size at approximately 14 Ma and has changed little since then. This hypothesis is supported by oceanic oxygen isotope records, cosmo-

* Corresponding author. Present address: Environmental Studies Program, Hobart and William Smith Colleges, Geneva, NY 14456, USA. Tel.: 315-781-3954; Fax: 315-781-3860.
E-mail addresses: ljoseph@hws.edu (L.H. Joseph), davidrea@umich.edu (D.K. Rea), vdpluijm@umich.edu (B.A. van der Pluijm), jdgleaso@umich.edu (J.D. Gleason).

0012-821X/02/$ – see front matter
PII: S0012-821X(02)00661-1

genic exposure ages, and ice sheet modeling (i.e. [10,13] and refs. therein). Others (i.e. [5,17]) have presented data that suggest the EAIS may have been wet-based and mobile during the Pliocene, when ice volumes may have decreased to as much as one-third of the present volume. Evidence of periods of extensive deglaciation is suggested by the presence of Pliocene diatoms in the Sirius Group, terrestrial flora and fauna, Antarctic margin drill hole data (i.e. Ross Sea), sedimentologic studies of Pliocene sections, seismic, and dust studies (i.e. [5,10,17,18]). The effect of climate warming, such as in the early Pliocene, on the extent of melting of the EAIS and on other potential climate system feedbacks remains uncertain. Summaries and issues of this debate are provided by Webb and Harwood [5], Sugden et al. [13], Kennett and Hodell [2], Wilson [9], Burckle et al. [8], and Miller and Mabin [10].

Here we report on the sediment record recovered at Ocean Drilling Program (ODP) Site 745, on the East Kerguelen Plateau sediment drift (59°36′S, 85°06′E, 4082 m water depth; Fig. 2) [19] in the southern Indian Ocean. We examine indications of Antarctic ice sheet stability, as well as fluctuations in the intensity of deep-water circulation, for the last 6.5 Myr, a timespan that includes the Pliocene warm interval. Our interpretations are based on the assumption that the nature and amount of sediment deposited at sites hundreds of kilometers seaward of the Antarctic margin are related to delivery of sediment to the ocean, and thus will reflect changes in physical erosion processes on Antarctica, as well as circulation in the surrounding ocean [20–22].

1.1. Background information and substantiation of study assumptions

1.1.1. Surface and deep oceanic circulation: a global heat conveyor

The Antarctic Circumpolar Current (ACC) is a strong clockwise ocean current that encircles Antarctica, transporting approximately $115–145\times10^6$ m^3/s of water [23]. It is important to global ocean heat transport as it isolates Antarctica from warm low-latitude surface waters while at the same time it enables the three major oceans to exchange water. Unlike most other surface water currents, the ACC extends to the ocean bottom around Antarctica, due to the lack of a distinct pycnocline. Hydrographic studies find the near-bottom path of the clockwise-flowing ACC to be altered by the presence of Kerguelen Plateau (Fig. 3). Most of the flow passes north of the Kerguelen Island, yet about a third flows across the plateau or through the Princess Elizabeth Trough, which separates Kerguelen Plateau from Antarctica. The water passing through the Princess Elizabeth Trough curls north around the southern flank of Kerguelen Plateau in response to the Coriolis force, before turning eastward once again [24–26].

Sediment drifts, such as the East Kerguelen Ridge sediment deposit, are constructed from sediment transported (and deposited) by the flow of bottom waters, and are characterized by relatively high sedimentation rates when compared to the normal deep-sea environment. Site 745 lies within the present-day Antarctic Bottom Water (AABW), which can reach flow velocities in excess of 15 cm/s (Figs. 2 and 3) [27].

1.1.2. Physical erosion of Antarctica: glacial sediment generation, discharge, and transport

Modes of sediment transport from the Antarctic continent and surrounding ocean to Kerguelen might include ice rafting, settling of biogenic grains, hemipelagic processes, turbidites, and bottom water current transport. However, Antarctic sediment must first be eroded and delivered to the continental margin before being transported out to the sea floor (Fig. 4A).

A review of field data by Hallet et al. [28], primarily reflecting the activity of mountain glaciers and glaciated basins (as opposed to ice sheets), provides insight into the relative timing and conditions of sediment erosion, transportation, and deposition in glaciated areas. Various factors cause sediment yields to vary substantially between similar basins. These factors include: (a) whether the glacier is cold-based and frozen to the bed with minimal basal sliding (basal sliding increases erosion); (b) sliding speed (faster speed increases erosion); (c) the size of the glacier (greater ice coverage, more erosion); (d) the ice

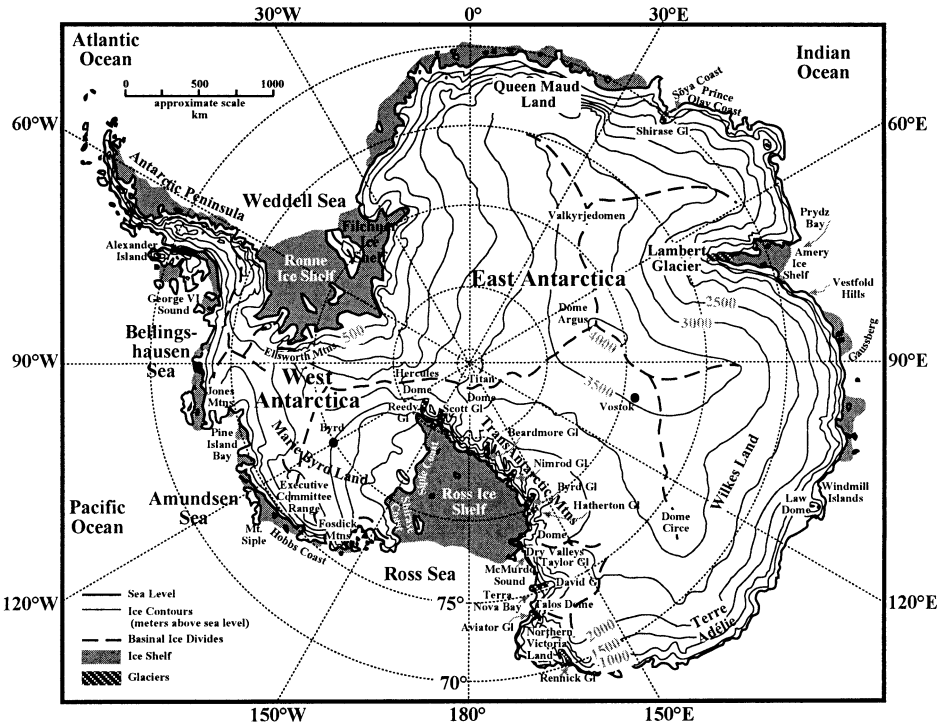

Fig. 1. Map of Antarctica. Adapted from Denton et al. [54].

flux; and (e) meltwater production and routing to the glacial terminus (which may include subaerial as well as subglacial processes). Greater amounts of both suspended sediment and bedload transport occur during times characterized by high water discharge that occurs over much of the melt season. Elevated erosion rates and major pulses of sediment delivery would be expected during significant glacial advances based on two assumptions: (a) that debris had collected in basins due to subaerial erosion during ice recessions and (b) that the debris is evacuated shortly after ice advance and deposited at or across the glacial margin [21]. Thus sediment yields from ice re-advance should be relatively high, yet should decrease once the ice sheet stabilizes.

Based on the work of Hallet et al. [28] and other studies [11,29–33], we suggest that if the EAIS extends over the continent, is stable and cold-based (i.e. frozen to the ground), little eroded material will be transported to and across the continental margin. However, if the EAIS is active and wet-based, the movement of the ice in addition to the outflow of meltwater will significantly increase the amount of material transported to the Southern Ocean. Hence, increased deep-sea terrigenous accumulation rates of sediment derived from Antarctica will reflect periods of instability of the EAIS.

1.2. Ice rafting

Ice rafting occurs when glaciers reach sea level and calve off from the main ice sheet to form icebergs. Debris is transported with the iceberg and as it melts, particles of all sizes fall into the sea. Production of ice-rafted debris (IRD) is a function of many factors, including the size of the ice sheet, erodability of the basal rock, thermal ice regime, ice flux to the grounding line, location of the grounding ice, and ice shelves. The distribution of IRD is influenced by circulation patterns and temperatures. Thus the detection of IRD indicates the presence of glacial ice

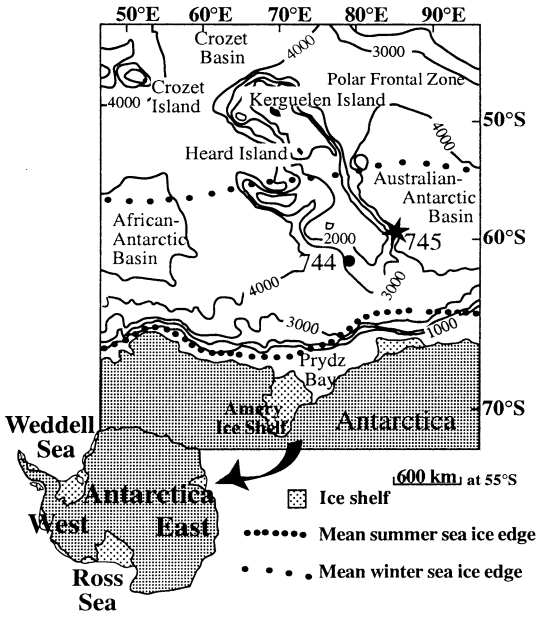

Fig. 2. Location map of key ODP Leg 119 Sites. Adapted from Ehrmann et al. [27].

at sea level [29]. The most favorable conditions for producing IRD are with melting/freezing base glaciers from valley or outlet settings. Any process (such as sea level rise) that lifts the ice margin from its bed, will result in catastrophic iceberg calving [27].

Kerguelen Plateau is located seaward and north of Prydz Bay and the Amery Ice Shelf. The northern Prince Charles Mountains overlook the western side of the Lambert Glacier that merges with the Amery Ice Shelf (Fig. 4). The Lambert Glacier Trough, formed as the Amery Ice Stream cut into underlying sediment at a time when the ice sheet extended beyond its present limits, extends out onto the continental shelf as the Prydz Bay Trough [11,32,34]. Eight major ice streams feed into the Amery Ice Shelf and it has been estimated that 32% of the ice volume reaching the shelf originated in the northern Prince Charles Mountains [32,35]. Most of the ice draining from Antarctica flows onto ice shelves, which are then the source of calved icebergs. The Amery Ice Shelf is one of the three largest ice shelves on Antarctica and serves to collect sediment from vast drainage basins and thus acts as a focused sediment outlet to the sea [31,32,34,35]. In addition, variations in the Lambert glacier system may be representative of fluctuations in the EAIS as a whole [11]. Fig. 4A provides current ice flow directions and basinal divides for Antarctica. Thus, the proximity of Kerguelen Plateau to Prydz Bay and the Amery Ice Shelf increases the likelihood of ODP Site 745 receiving a sedimentary signature of Antarctic climate variations.

Ehrmann et al. [27] studied ice rafting on the

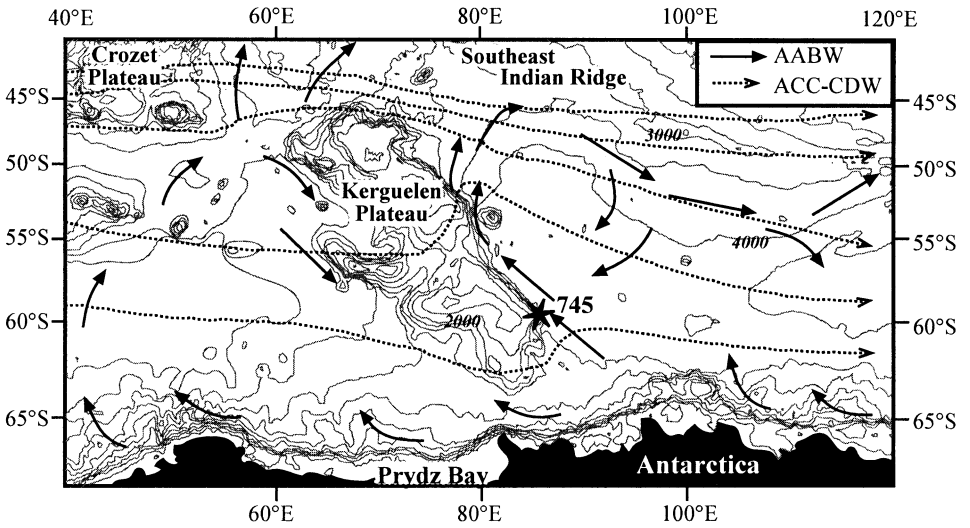

Fig. 3. ACC and AABW flow around Kerguelen Plateau. Adapted from Dezileau et al. [26].

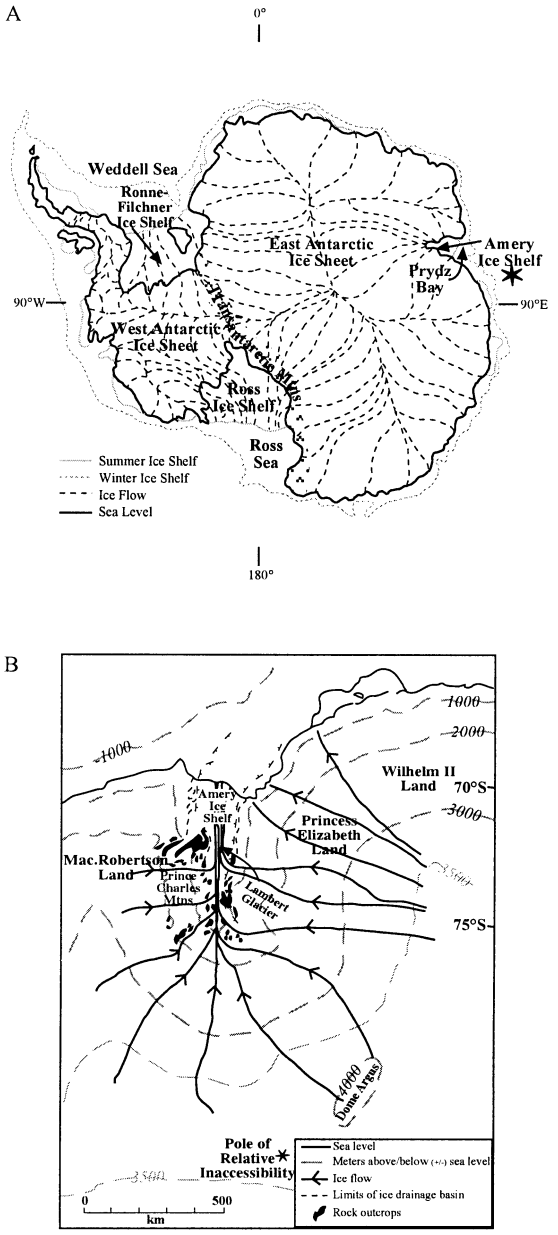

Fig. 4. (A) Map of glacial drainage from Antarctica. The star represents the estimated location of Site 745. Adapted from Anderson [55]. (B) Amery ice shelf area. Adapted from Hambrey [35].

Kerguelen Plateau by examining the grain size and lithology of sediment from both ODP Sites 745 and 746 (about 5 km away from Site 745). These data provide the timing and relative magnitude of ice-rafting events detected at Kerguelen Plateau over the last 10 Ma. The presence of IRD is indicated by an increase in the amount of terrigenous sand (between 2 mm and 63 μm) and gravel (>2 mm). The lithologies of the IRD (granitic and gneissic), as well as the clay mineralogy, indicate an East Antarctic origin [27]. The

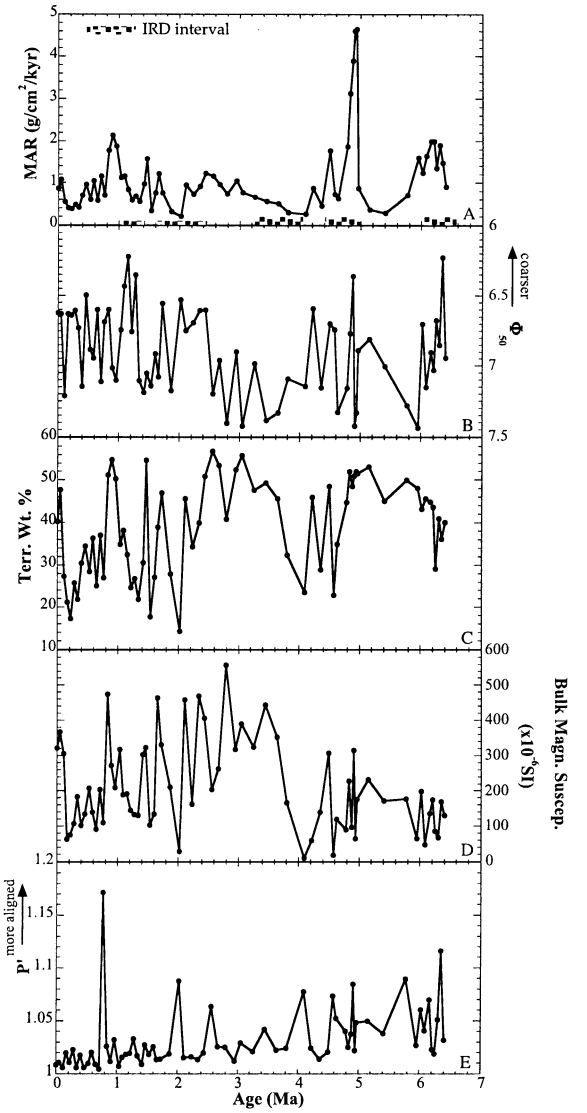

Fig. 5. Results of sediment characterization for Site 745. Terrigenous MAR, grain size, weight percent, bulk magnetic susceptibility and magnetic fabric intensity. Ice-rafting intervals as noted by Ehrmann et al. [27]; the larger boxes indicate more intense intervals.

Table 1
ODP Leg 119, Site 745 age datums used for linear extrapolation of sample ages (depths of chrons from Barron et al. [39] and ages from Cande and Kent [40])

Depth (mbsf)	Age (Ma)
42.48	0.78
91.55	1.77
93.55	1.95
112.6	2.581
123.6	3.04
125.6	3.11
126.6	3.22
128.6	3.33
133.1	3.58
142.7	4.18
146.3	4.29
149.4	4.48
156.1	4.62
160.8	4.8
167.9	4.89
177.9	4.98
180.7	5.23
186.4	5.89
196.7	6.14
205.7	6.27

timing and relative magnitude of these episodes are indicated in Fig. 5.

Here we investigate the variability of ice coverage on Antarctica during the latest Miocene through Pleistocene time. Variability would be indicated primarily in large shifts in the mass accumulation rates (MARs) of Antarctic sediment deposited at Kerguelen Plateau. Through the use of grain alignment and terrigenous grain size, we also investigate the relative strength and variability in the currents that influence this sediment drift site.

2. Methods

2.1. Terrigenous sediment characterization

Sixty-eight separate samples of the Kerguelen drift (adjacent scoop samples and $2.2\times2.1\times1.4$ cm paleomagnetic cubes) were obtained from ODP Site 745. Sampling density, intended to detect long-term changes, is approximately one sample every 100 ky and is thus too low a resolution to decipher glacial–interglacial variability or detect short-term climatic extremes. Scoop samples were subject to a chemical extraction process based on procedures described by Rea and Janecek [36], with modifications by Clemens and Prell [37] and Hovan [38]. This process removes calcium carbonate, oxides and hydroxides, zeolites, and biogenic silica in order to isolate the terrigenous mineral component of marine sediment. The terrigenous weight percent is calculated by comparing the weight of each sample before and after chemical extraction. The age model is based on paleomagnetic data [39] with the ages of the chrons taken from the timescale of Cande and Kent [40] (Table 1).

MARs of the terrigenous sediment component (in g/cm^2/kyr) were calculated using the equation:

$$\text{Terrigenous MAR} = \text{LSR}\times\text{DBD}\times \text{terrigenous weight percent}/100$$

where LSR is the linear sedimentation rate (in cm/kyr) determined from the reversal timescale on this core, DBD is the dry bulk density (in g/cm^3) obtained from shipboard bulk density values, and the terrigenous weight percent is determined using the chemical extraction method provided above. As a result, the interpretation of terrigenous input is independent of dilution/concentration effects incurred by variations in input rates of other sediment components. For time periods with a constant LSR, the terrigenous MAR is primarily driven by terrigenous weight percent.

Grain size analysis was performed on the extracted terrigenous component using a Multisizer IIE Coulter Counter with a chosen analysis range from 2 to 50 μm, according to the methodology presented by Rea and Hovan [41]. Terrigenous median grain size is represented here in both microns and Φ_{50} ($\Phi = -\log_2(\text{grain diameter}_{\text{mm}})$).

2.2. Isotopic analyses

Isotopic analyses of Pb, Sr and Nd were obtained for 10 samples of the extracted terrigenous fraction from Site 745. Samples were digested in savillex beakers on hotplates using a combination

Table 2
Sediment analysis results of samples from ODP Site 745

Core	Samp top (cm)	Samp bot (cm)	Samp depth (mbsf)	Extrap age (Ma)	Terrig wt% (%)	Terrig MAR (g/cm^2/kyr)	Ave. terrig. grain size data 50th%				Bulk mag suscep ($\times 10^{-6}$ SI)	P'
							50th% (μm)	S.D. (μm)	50th% (Φ)	S.D. (Φ)		
1H2	78	80	2.28	0.00	40.25	0.87	10.14	9.21	6.62	1.07	321	1.01
1H4	25	27	4.75	0.05	47.71	1.09	10.10	9.43	6.63	0.94	366	1.01
2H2	126	128	7.76	0.11	27.26	0.55	6.73	7.93	7.21	1.02	305	1.01
2H4	125	127	10.75	0.16	21.14	0.40	10.09	9.16	6.63	1.01	63	1.02
2H6	90	92	13.40	0.22	17.21	0.38	10.02	9.23	6.64	1.12	75	1.01
3H2	76	78	16.76	0.28	25.71	0.47	10.26	10.13	6.61	1.14	107	1.02
3H4	75	77	19.75	0.34	21.87	0.41	9.41	10.15	6.73	1.29	183	1.01
3H6	66	68	22.66	0.40	30.43	0.70	7.07	8.73	7.14	0.97	102	1.02
4H2	42	44	25.92	0.46	34.44	0.95	11.09	9.69	6.50	1.08	134	1.01
4H4	90	92	29.40	0.53	28.38	0.60	8.49	9.25	6.88	1.08	208	1.01
4H6	80	82	32.30	0.58	36.31	1.05	8.12	8.38	6.94	0.93	140	1.02
5H2	67	69	35.67	0.65	25.07	0.57	10.30	10.24	6.60	1.18	90	1.01
5H4	90	92	38.90	0.71	37.02	1.16	7.22	8.31	7.11	1.11	203	1.00
5H6	67	69	41.67	0.76	26.91	0.71	9.75	10.32	6.69	1.18	110	1.17
6H2	76	78	45.26	0.84	51.12	1.77	10.32	9.51	6.60	1.09	474	1.03
6H4	76	78	48.26	0.90	54.71	2.13	7.74	8.04	7.01	0.99	271	1.01
6H6	82	84	51.32	0.96	50.31	1.87	7.29	8.40	7.10	1.04	208	1.03
7H2	123	125	55.23	1.04	34.91	1.12	9.33	9.61	6.74	1.10	317	1.01
7H4	85	87	57.85	1.09	38.13	1.15	11.58	9.97	6.43	1.07	189	1.02
7H6	77	79	60.77	1.15	32.39	0.83	13.40	11.14	6.22	1.19	192	1.02
8H2	65	67	64.15	1.22	24.60	0.60	9.27	9.71	6.76	1.15	144	1.02
8H4	74	76	67.24	1.28	26.77	0.68	12.25	10.82	6.35	1.24	133	1.03
8H6	78	80	70.28	1.34	21.78	0.55	7.27	8.82	7.10	1.16	130	1.02
9H2	94	96	73.94	1.41	30.52	0.97	6.85	8.62	7.19	1.09	303	1.01
9H4	41	43	76.41	1.46	54.63	1.57	7.54	7.61	7.05	0.98	323	1.03
9H6	85	87	79.85	1.53	17.69	0.33	7.08	9.59	7.14	1.22	103	1.02
10H2	93	95	83.43	1.61	27.03	0.76	8.29	9.17	6.92	1.07	133	1.03
10H4	66	68	86.16	1.66	38.92	1.22	7.40	8.26	7.08	1.05	464	1.01
10H6	42	44	88.92	1.72	46.96	0.75	10.63	10.07	6.56	1.05	331	1.01
11H2	66	68	92.66	1.87	27.84	0.31	6.92	8.15	7.18	1.08	210	1.02
11H4	69	71	95.69	2.02	14.24	0.20	10.83	10.03	6.53	1.05	28	1.09
11H6	42	44	98.42	2.11	45.55	0.95	9.28	9.85	6.75	1.19	458	1.02
12H2	64	66	102.14	2.24	34.32	0.72	9.71	10.51	6.69	1.26	162	
1.02												
12H4	94	96	105.44	2.34	39.85	0.91	10.26	10.09	6.61	1.21	469	1.01
12H6	68	70	108.18	2.44	50.85	1.22	10.29	9.74	6.60	1.05	405	1.02
13H2	93	95	111.93	2.56	56.75	1.16	6.80	8.10	7.20	1.07	204	1.06
13H4	58	60	114.58	2.67	53.43	0.96	8.03	8.96	6.96	1.06	262	1.03
13H6	65	67	117.65	2.79	40.78	0.74	5.89	7.13	7.41	1.00	557	1.03
14H2	92	94	121.42	2.95	52.42	1.05	8.37	8.49	6.90	1.02	317	1.01

Table 2 (*Continued*)

Core	Samp top (cm)	Samp bot (cm)	Samp depth (mbsf)	Extrap age (Ma)	Terrig wt% (%)	Terrig MAR (g/cm^2/kyr)	Ave. terrig. grain size data 50th%				Bulk mag suscep ($\times 10^{-6}$ SI)	P'
							50th% (μm)	S.D. (μm)	50th% (Φ)	S.D. (Φ)		
14H4	35	37	123.85	3.05	55.71	0.77	5.81	7.40	7.43	0.99	390	1.03
14H6	57	59	127.07	3.25	47.63	0.66	7.92	8.80	6.98	0.97	323	1.02
15H2	63	65	130.63	3.45	49.30	0.56	5.98	8.73	7.39	1.20	442	1.04
15H4	102	104	134.02	3.64	45.61	0.50	6.20	7.70	7.33	1.00	353	1.02
15H6	66	68	136.66	3.80	32.34	0.29	7.33	8.60	7.09	1.09	166	1.02
17H2	78	80	141.28	4.09	23.51	0.26	7.06	8.27	7.15	1.09	9	1.08
17H4	35	37	143.85	4.21	45.86	0.87	10.37	9.45	6.59	0.96	59	1.02
17H6	85	87	147.35	4.35	28.90	0.44	7.01	8.58	7.16	1.14	139	1.01
18H2	14	16	150.14	4.49	48.44	1.76	9.60	9.13	6.70	0.98	306	1.02
18H4	81	83	153.81	4.57	22.81	0.73	9.33	9.59	6.74	1.20	18	1.07
18H6	30	32	156.30	4.63	34.83	0.62	6.22	7.14	7.33	0.89	118	1.05
19H2	83	85	160.33	4.78	44.68	1.86	7.01	8.20	7.16	0.94	89	1.04
19H4	65	67	163.15	4.83	51.94	3.12	9.16	9.05	6.77	1.02	227	1.02
19H6	128	130	166.78	4.88	48.47	3.89	12.15	10.49	6.36	1.08	96	1.04
20H2	90	92	169.90	4.91	50.90	4.60	5.84	8.18	7.43	1.03	315	1.08
20H4	118	120	173.18	4.94	51.89	4.64	6.20	7.87	7.33	1.02	64	1.02
20H6	82	84	175.82	4.96	51.52	0.87	8.43	8.69	6.89	1.03	175	1.05
21H2	135	137	179.85	5.15	53.11	0.36	8.92	9.54	6.81	1.10	232	1.05
21H4	75	77	182.25	5.41	45.06	0.28	7.79	9.00	7.01	1.20	171	1.04
21H6	84	86	185.34	5.77	49.92	0.71	6.43	8.29	7.28	1.06	177	1.09
22H2	82	84	188.82	5.95	48.02	1.59	5.76	7.22	7.44	0.95	64	1.03
22H4	65	67	191.65	6.02	43.14	1.24	9.59	9.52	6.70	1.06	198	1.06
22H6	29	31	194.29	6.08	45.60	1.64	7.04	8.10	7.15	0.94	47	1.04
23H2	79	81	198.29	6.16	44.77	1.98	8.34	8.59	6.91	0.98	136	1.07
23H4	71	73	201.21	6.20	43.62	1.99	7.65	7.76	7.03	0.97	174	1.02
23H6	42	44	203.92	6.24	29.06	1.35	9.77	9.70	6.68	1.13	85	1.02
24H2	64	66	207.64	6.30	40.88	1.89	8.63	8.97	6.86	1.05	67	1.05
24H4	93	95	210.93	6.35	36.12	1.48	13.35	11.71	6.23	1.22	168	1.12
24H6	144	146	214.44	6.40	40.00	0.90	8.11	9.35	6.95	1.20	129	1.03

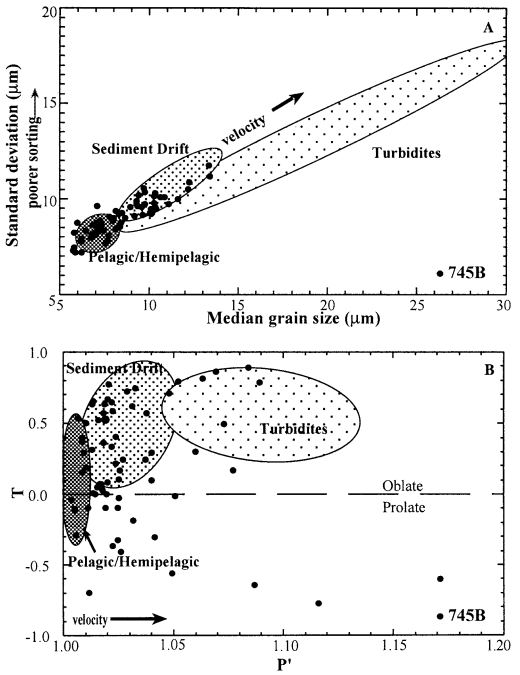

Fig. 6. Environmental energy classification. (A) Terrigenous median grain size versus standard deviation and (B) magnetic fabric (P') versus ellipsoid shape (T). The black dots give the results from ODP Site 745B samples, while the larger shaded areas behind them indicate previously defined energy fields [22]. The pelagic/hemipelagic field indicates a low energy depositional environment, the sediment drift field indicates a moderate energy, and the turbidite field indicates a high energy environment. The combination of magnetic fabric and grain size information indicates a moderate (sediment drift) depositional environment for ODP Site 745B.

of HF, HNO_3 and $HClO_4$ acids. Nd separation was performed by conventional cation exchange (REE), followed by reverse phase (HDEHP) chromatography for separation of Nd and Sm. Sr was separated on miniaturized Sr-Spec columns. Isotopic compositions of Sr and Nd were measured in static mode on a Finnigan 262 thermal ionization mass spectrometer. Pb isotopic compositions were obtained without chemical separation using a sample-standard bracketing technique (B. Klaue, pers. commun.) on a Finnigan Element magnetic sector single collector ICP-MS.

2.3. Magnetic fabric analysis

Anisotropy of magnetic susceptibility (AMS) was measured on the paleomagnetic cubes using a KLY-2 KappaBridge. Results of AMS analyses show the bulk orientation of all grains in a sample, called the magnetic fabric, and are represented in three-dimensional space by an ellipsoid; in most cases the greatest induced magnetization parallels the long axis [42,43]. The parameter P' mathematically represents the degree of anisotropy of the resulting magnetization ellipsoid (greater P' values represent a more developed anisotropy of the magnetization ellipsoid) and parameter T represents the shape factor of the ellipsoid. When $0 < T \leq 1$, then the ellipsoid is oblate while if $-1 \leq T < 0$, the ellipsoid is prolate.

Previous studies have provided robust methods by which the mode of terrigenous sediment transport and depositional processes can be determined by appropriate analyses of a single sample using a combination of AMS and terrigenous grain size analyses. Hemipelagic and eolian grains display random orientation and different size distributions; drifts and distal turbidites have a pronounced fabric and different size distribution patterns [22,41,44].

3. Results

Terrigenous MAR values for Site 745 generally range from ~0.5 to 2 g/cm^2/kyr with the greatest values extending to nearly 5 g/cm^2/kyr at approximately 4.9 Ma (Table 2, Fig. 5A). Ice-rafting intervals (from [27]) younger than ~4 Ma generally correspond to times of relatively low terrigenous MAR. Prior to ~4 Ma, the intervals of high MAR correspond to intervals of ice rafting. Median terrigenous grain size values range from 7.5 to 6.2Φ (5.52–13.6 μm). Finer grains occur in the interval between approximately 2.6 and 4 Ma and most coarse size peaks are contained within episodes of ice rafting (Fig. 5B). The youngest interval (present to 2.6 Ma) is overall slightly coarser than the oldest interval (4–6.5 Ma). The terrigenous weight percent (Fig. 5C), derived from the chemical extraction process, shows moderate variation throughout (~25–60%) and no distinctive change at 4 or 2.6 Ma.

Bulk magnetic susceptibility values range from

Table 3
Isotopic results from Site 745

Samp. depth (mbsf)	Extrap. age (Ma)	$^{204}Pb/^{206}Pb$	$^{207}Pb/^{206}Pb$	$^{208}Pb/^{206}Pb$	$^{87}Sr/^{86}Sr$	ε_{Nd}
22.66	0.40	0.0556	0.8692	2.1627	0.73606	−17.2
48.26	0.90	0.0558	0.8727	2.1704	0.73727	−18.8
92.66	1.87	0.0549	0.8599	2.1418	0.72668	−9.2
108.18	2.44	0.0549	0.8612	2.1401	0.72757	−15.9
123.85	3.05	0.0555	0.8679	2.1649	0.73205	−15.7
134.02	3.64	0.0554	0.8678	2.1698	0.73361	−16.8
147.35	4.35	0.0558	0.8699	2.1542	0.73136	−13.1
173.18	4.94	0.0554	0.8689	2.1663	0.73761	−18.5
182.25	5.41	0.0555	0.8677	2.1488	0.73734	−14.4
201.21	6.20	0.0554	0.8702	2.1707	0.73899	−19.4

20 to 600×10^{-6} SI. There is an important transition in the character of the curve at approximately 4 Ma (Fig. 5D). Susceptibility values slowly increase and become more irregular from 0 to 3.4 Ma until a rapid decrease in strength occurs between ~3.4 and 4 Ma. Susceptibility values are relatively low for the remainder of the record. P', the strength of the magnetic fabric (Fig. 5E), ranges from 1.01 to 1.1, with a one-point high at 1.17, and exhibits a general increasing trend downcore, with an increased frequency of major P' peaks older than approximately 3.9 Ma.

Site 745 sediment characteristics are compared to those of previously defined environmental energy fields in Fig. 6 [22]. The pelagic/hemipelagic field on this diagram indicates a low energy depositional environment, the sediment drift field indicates a moderate energy environment, and the turbidite field indicates a high energy environment. The 745 samples fall within the sediment drift/middle and pelagic–hemipelagic/lower depositional energy fields for grain size (Fig. 6A) and the sediment drift/middle depositional energy field magnetic fabric (Fig. 6B).

Results of the isotopic analyses show a crude co-variation with each other, and the ε_{Nd} plot appears to follow the MAR curve (Table 3; Fig. 7). ε_{Nd} values range from approximately −6 to −19 while $^{87}Sr/^{86}Sr$ ratios fall between 0.726 and 0.740. In Fig. 8, ε_{Nd} and $^{87}Sr/^{86}Sr$ values for East Antarctica, Kerguelen Plateau, Patagonia and ODP Site 745 are shown to illustrate provenance of the Site 745 samples [45].

4. Discussion

4.1. Terrigenous MARs, IRD, and provenance: stability of the ice sheet

The rate of accumulation of terrigenous sediment in the East Kerguelen Ridge sediment drift is relatively large (Fig. 9A), often more than 1 g/cm^2/kyr and ranging up to ~4.6 g/cm^2/kyr. Typical non-drift deep-sea terrigenous MARs average about 0.5 to 2–3 g/cm^2/kyr for hemipelagic muds and ten to hundreds of mg/cm^2/kyr for eolian dust [20]. The higher MAR values, which occur at 6.4–5.9, 4.9–4.6, and 1.0–0.8 Ma, denote a greater sediment flux and display isotopic values of the terrigenous material consistent with an Antarctic source region. These data therefore imply an Antarctic ice sheet with greater meltwater production/glacial sediment erosion on Antarctica than would occur with a stable, cold-based ice sheet [28,29].

An active ice sheet (waxing and waning) that extends to the continental margin results in the most favorable conditions for producing IRD [27]. Thus, the more intense periods of ice rafting that occur prior to 4 Ma and are coincident with the MAR peaks, also imply extensive, but less stable, ice coverage on Antarctica (Fig. 9A). Ehrmann et al. [27] also suggest that variations in ice

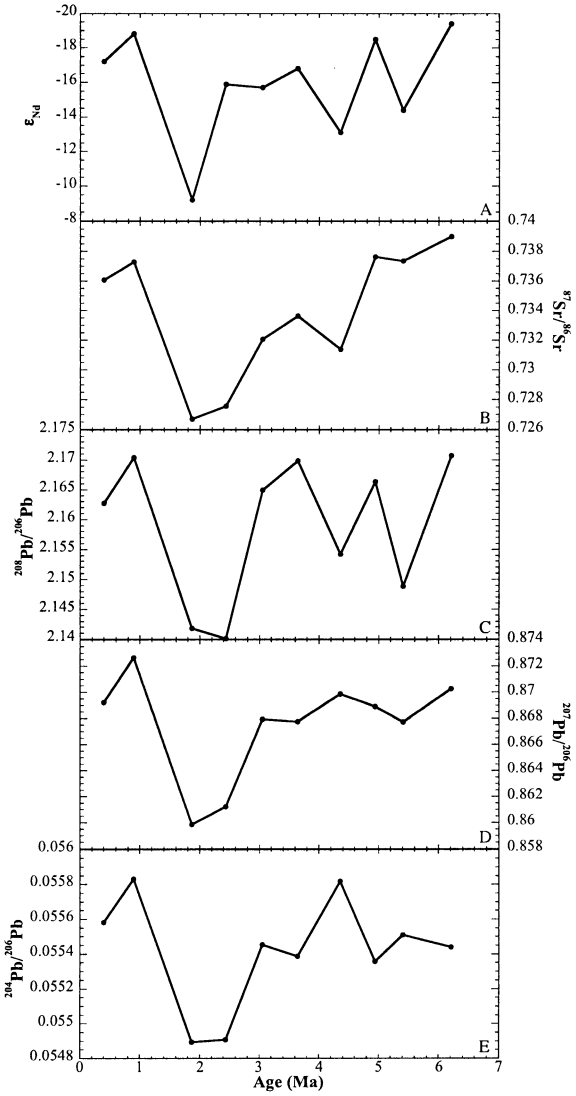

Fig. 7. Results of isotopic analysis of Pb, Sr, and Nd for Site 745.

sheet grounding location and sediment storage, in addition to lower sea level low-stands, likely resulted in the smaller amounts of IRD detected in the younger part of the record. These variations (or possibly changes in circulation patterns) may also account for the lack of correspondence of the periods of ice rafting and high MARs during this time period.

Overall, the isotopic analyses of the terrigenous grains indicate a minor background component of Kerguelen Plateau basalt composition with a superimposed continental East Antarctic composition signal (Figs. 7 and 8) [45]. Terrigenous MARs and negative ε_{Nd} values (Fig. 9A) follow a similar pattern. Thus, MAR peaks correspond to times in which a greater amount of Antarctic-derived sedimentation occurs, providing strong support for our assumption that times of the rapidly accumulating sediment indeed represent periods of enhanced Antarctic continental erosion and delivery of sediment to the deep sea.

Together, the MARs, IRD flux, and geochem-

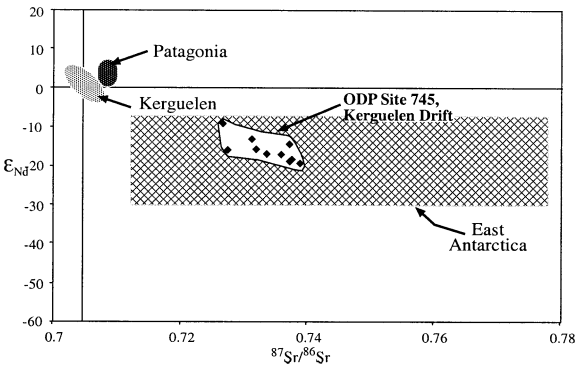

Fig. 8. Nd–Sr isotope correlation diagram showing various isotopic provenance fields for Kerguelen Plateau basalts and Indian Ocean basalts [56], Patagonian loess and East Antarctic basement data [57].

istry are consistent with an – at least intermittently – wet-based and active ice sheet present prior to ~4 Ma. Although the extent of this variability has not been determined by this study, this interpretation of latest Miocene and early Pliocene ice sheet activity is supported elsewhere, in many different manners. A study on southern Kerguelen Plateau ODP Site 751 by Breza [46] mentions a possible deglaciation of the EAIS between 4.5 Ma and 4.1 Ma that would have resulted in the release of large amounts of IRD into the Southern Ocean. Bohaty and Harwood [47] determine a peak warming event of the southern Kerguelen Plateau surface water, likely related to shifting of the polar front, at ~4.3 Ma, with smaller warm events occurring at ~4.5 and ~3.6 Ma. A study of the Pagodroma Group of the Lambert Glacier during Miocene and Pliocene times by Hambrey and McKelvey [11,32] presents evidence of a dynamic Neogene Antarctic Ice Sheet, varying considerably in volume, with the sliding glaciers carrying large amounts of basal and supraglacial debris. In their studies of Vestfold Hills (Sørsdal Formation; Fig. 1), Whitehead et al. [48] indicate that the period between 4.5 and 4.1 Ma is warmer than the present. Bart [12] provides evidence that during the early Pliocene, despite times of overall, global ice-volume reduction, Antarctic ice volumes may have increased to larger than present levels. Ice volume curves constrained by Mg/Ca paleotemperature informa-

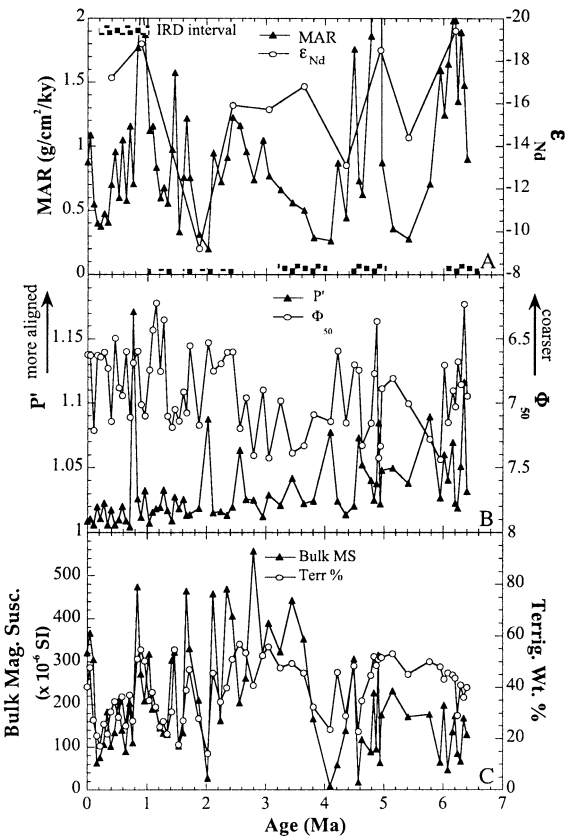

Fig. 9. Paleoenvironmental proxy indicators from ODP Hole 745B. (A) Terrigenous mass accumulation rates and ε_{Nd} versus age. Ice-rafting intervals as noted by Ehrmann et al. [27]; the larger boxes indicate more intense intervals. Note the three major episodes of sediment accumulation correlate to more negative values of ε_{Nd}. Prior to 4 Ma, ice-rafting intervals also correlate to times of high MAR, which is not true in younger periods. (B) Magnetic fabric (P') and terrigenous median grain size (Φ_{50}) versus age. P' shows a decreasing trend throughout the entire time period, while the Φ_{50} values exhibit a finer interval between around 4 and 2.6 Ma. (C) Bulk magnetic susceptibility and terrigenous weight percent versus age. These two factors vary together at times older than 4.3 and younger than 2.3 Ma. Note the relatively small variation in terrigenous weight percent (times two) while the bulk magnetic susceptibility values (often used as an indicator of terrigenous input) show large variability (times 30). This is particularly noticeable at ~4 Ma, where the bulk magnetic susceptibility exhibits its largest change which is not coincident in the terrigenous weight percent.

tion in benthic foraminiferal calcite compiled by Lear et al. [49] exhibit at least two large reductions in ice volume between the major ice sheet expansion at 14 Ma and northern hemisphere gla-

ciation at approximately 2.6 Ma (~11–9 and 5–3 Ma). Based on our data, another episode of wet-based ice on Antarctica also occurred between 1.1 and 0.8 Ma and is possibly related to the period of warmth and variable ice conditions noted in studies from the Cape Roberts Project (CRP-1; e.g. [50,51]). In general, this study supports the conclusions of Barker [6], a study which notes significant variations in early Pliocene Antarctic climate, but does not find evidence for extensive deglaciations during the early Pliocene, an alternative explanation to the extremes of the early Pliocene EAIS stability debate.

Interestingly, these results indicate that a more stable and cold-based ice sheet established itself during the middle of the Pliocene warm interval, although discrete, short-term events may not be detected due to the sampling resolution of this study. Bart [12] mentions periods of ice growth during warmer time periods and associates the ice growth with an increased amount of precipitation due to the higher evaporation associated with increased temperatures, an explanation advanced by Ruddiman and McIntyre [52] for the growth of northern hemisphere sheets.

4.2. Anisotropy and median grain size: bottom water velocity variation

The degree of anisotropy of magnetic susceptibility, represented here by P', is a measure of the non-uniformity of the magnetic susceptibility with direction. The non-spherical shape of the resultant magnetic field is a function of many things, primarily mineralogy combined with grain alignment. An increase in both P', representing the degree of magnetic anisotropy, or strength of fabric, and median terrigenous grain size correlates with an increase in interpreted depositional energy; as current velocity increases, more grains will align with each other and stronger currents can support larger grains (Fig. 6). These combined results indicate the influence of bottom water flow upon deposition. The combination of magnetic fabric and grain size information for ODP Site 745 indicates a predominantly middle-range (sediment drift) depositional energy environment (Fig. 6).

The greater values of P' and coarser median grain sizes at times older than 4 Ma indicate that a stronger, more variable, deep-water current was present (Fig. 9B). The relatively fine-grained interval between 4 and 2.6 Ma with decreasing and less variable P' values indicates a decrease in current velocities/influence at this time. Within the youngest interval, low P' values indicate a diminished current influence, even though grain size is somewhat larger, probably an effect of changing sediment source or transport distance.

As mentioned above, magnetic fabric can be a function of a number of things unrelated to current velocity. However, the lack of a linear relationship of P' with shipboard bulk density measurements ($r^2 = 0.4$) indicates that the increase of P' with depth is not simply a result of compaction. In addition, P' is highest when the bulk magnetic susceptibility is low (at times older than 4 Ma), indicating that the relatively high P' values do not result from a change in the magnetic mineralogy. Also, high P' values do not always occur during ice-rafting intervals, belying the concern that P' value peaks were caused by one large ice-rafted grain.

4.3. Magnetic susceptibility and terrigenous weight percent: changes in oceanic circulation patterns

Fig. 9C shows the variation of bulk magnetic susceptibility and terrigenous weight percent. As bulk magnetic susceptibility is often an indicator of terrigenous input, the curves should, in general, co-vary in magnitude and timing. However, the terrigenous weight percent shows relatively little variation throughout (~25–60%) when compared with the larger range in susceptibility values (change over an order of magnitude). This is especially noticeable at the largest change in bulk susceptibility at approximately 4 Ma, where there is no equivalent variation in terrigenous weight percent. These curves co-vary during intervals younger than ~2.3 Ma and older than ~4.2 Ma.

The lack of co-variance of the bulk magnetic susceptibility and terrigenous weight percent curves in the period between 4.3 and 2.3 Ma, as well as the differences in the range of values for

the two curves (20–600$\times 10^{-6}$ SI and 25–60%, relatively), especially at the sharp change of bulk susceptibility at ~4 Ma, indicate that some factor other than terrigenous weight percent is influencing the bulk magnetic susceptibility signal between 4.3 and 2.3 Ma. This might indicate a change in magnetic mineralogy at this time, rather than in amount of terrigenous input. This hypothesis is supported by low-temperature experiments [53] on selected samples. This test indicates that the paramagnetic versus ferrimagnetic contents are clearly different before and after 4 Ma, with the paramagnetic minerals more dominant prior to 4 Ma (i.e. more clay-rich). Additionally, the greater input of Kerguelen Plateau basaltic material, as indicated by the less radiogenic isotopic composition of Sr and Pb (Fig. 7) [45] occurs between 4.4 and 1.9 Ma and supports the concept of a change in the relative supply of Kerguelen versus Antarctic materials to Site 745 as suggested by the bulk magnetic susceptibility and terrigenous weight percent data.

5. Summary and conclusions

In summary, the major findings of this study are:

1. The EAIS stabilized (~4 Ma) during the middle of the Pliocene warm interval (~4.8–3.2 Ma). However, discrete, short-term events are not likely to be noted this study.
2. EAIS activity is indicated by three episodes of high MAR of Antarctic derived material in the latest Miocene, earliest Pliocene, and middle Pleistocene.
3. A distinct change in all physical discriminators occurred at approximately 4 Ma.
4. The magnetic fabric indicates that variable velocity bottom currents occurred at times older than 4 Ma; however, overall, the strength of bottom water/drift currents declined through the entire interval (6.5 Ma–present).
5. A somewhat different sediment transport pattern may have occurred between 4 and 2.3 Ma, resulting in a different relative supply of sediment, as indicated by the grain size, terrigenous weight percent/bulk magnetic susceptibility, and geochemistry.

Overall, these results imply variable ice conditions on Antarctica in the latest Miocene and earliest Pliocene, which then progressed, in more recent times, to more stable ice conditions (excluding discrete, short-term fluctuations). Moderate deep-water current intensities have declined since 6.5 Ma and a change in the sediment supply pattern may have occurred between approximately 4.3 and 2.3 Ma. The EAIS became stable during a recognized Pliocene period of global warmth.

Acknowledgements

Many helpful comments were provided by Ted Moore, Josep Pares, Eric Steig, and Don Zak. We appreciate the insightful reviews and comments by David Harwood, Peter Barker, and an anonymous reviewer. Paula Weiss aided in obtaining samples from the ODP repository at Lamont-Doherty Earth Observatory. We thank Joel Blum, Bjorn Klaue and Andrea Klaue of the Michigan Radiogenic Isotope Geochemistry Laboratory for their assistance with the isotopic analyses. This research was based on samples and data provided by the Ocean Drilling Program (ODP). ODP is sponsored by the US National Science Foundation (NSF) and participating countries under management of Joint Oceanographic Institutions (JOI), Inc. This project was supported by NSF Office of Polar Programs grant No. OPP-9527067.*[SK]*

References

[1] J.H. Mercer, West Antarctic ice sheet and CO_2 greenhouse effect: a threat of disaster, Nature 271 (1978) 321–325.
[2] J.P. Kennett, D.A. Hodell, Stability or instability of Antarctic ice sheets during warm climates of the Pliocene? GSA Today 5 (1995) 1, 10–13, 22.
[3] R.A. Bindschadler, R.B. Alley, J. Anderson, S. Shipp, H. Borns, J. Fastook, S. Jacobs, C.F. Raymond, C.A. Shuman, What is happening to the West Antarctic Ice Sheet?, Eos 257 (1998) 264–265.

[4] R.P. Scherer, A. Aldahan, S. Tulaczyk, G. Possnert, H. Engelhardt, B. Kamb, Pleistocene collapse of the West Antarctic Ice Sheet, Science 281 (1998) 82–85.
[5] P.-N. Webb, D.M. Harwood, Late Cenozoic glacial history of the Ross Embayment, Antarctica, Quat. Sci. Rev. 10 (1991) 215–223.
[6] P.F. Barker, The proximal marine sediment record of Antarctic climate since the late Miocene, ARS 68 (1995) 25–57.
[7] L.H. Burckle, N.J. Potter, Pliocene-Pleistocene diatoms in Paleozoic and Mesozoic sedimentary and igneous rocks from Antarctica: a Sirius problem solved, Geology 24 (1996) 235–238.
[8] L.H. Burckle, A.P. Stroeven, C. Bronge, U. Miller, A. Wasell, Deficiencies in the diatom evidence for a Pliocene reduction of the East Antarctic Ice Sheet, Paleoceanography 11 (1996) 379–389.
[9] G.S. Wilson, The Neogene East Antarctic ice sheet: a dynamic or stable feature?, Quat. Sci. Rev. 14 (1995) 101–123.
[10] M.F. Miller, M.C.G. Mabin, Antarctic Neogene landscapes – In the refrigerator or in the deep freeze?, GSA Today 8 (1998) 1–3.
[11] M.J. Hambrey, B. McKelvey, Major Neogene fluctuations of the East Antarctic ice sheet: stratigraphic evidence from the Lambert Glacier region, Geology 28 (2000) 887–890.
[12] P.J. Bart, Did the Antarctic ice sheets expand during the early Pliocene?, Geology 29 (2001) 67–70.
[13] D.E. Sugden, D.R. Marchant, G.H. Denton, The case for a stable East Antarctic ice sheet; the background, Geogr. Annu. Ser. A 75 (1993) 151–154.
[14] J.P. Kennett, P. Vella, Late Cenozoic planktonic foraminifera and palaeoceanography at DSDP Site 284 in the cool subtropical south Pacific, Init. Rep. DSDP 29, 1975, pp. 887–890.
[15] T.J. Crowley, Modeling Pliocene warmth, Quat. Sci. Rev. 10 (1991) 275–282.
[16] R.Z. Poore, L.C. Sloan, Introduction: climates and climate variability of the Pliocene, Mar. Micropaleontol. 27 (1996) 1–2.
[17] M.J. Hambrey, P.J. Barrett, Cenozoic sedimentary and climatic record, Ross Sea region, Antarctica, ARS 60 (1993) 91–124.
[18] D.M. Harwood, P.-N. Webb, Glacial transport of diatoms in the Antarctic Sirius Group: Pliocene refrigerator, GSA Today 8 (1998) 1, 4–8.
[19] J. Barron, B. Larson, Scientific Staff of ODP Leg 119, Proc. ODP, Initial Results, Ocean Drilling Program 119, College Station, TX, 1989, 942 pp.
[20] D.K. Rea, Geologic records in deep sea muds, GSA Today 3 (1993) 205, 208–210.
[21] D.K. Rea, H. Snoeckx, Sediment fluxes in the Gulf of Alaska: paleoceanographic record from Site 887 on the Patton-Murray Seamount platform, Proc. ODP, Scientific Results, Ocean Drilling Program 145, College Station, TX, 1995, pp. 247–256.
[22] L.H. Joseph, D.K. Rea, B.A. van der Pluijm, Use of grain size and magnetic fabric analyses to distinguish among depositional environments, Paleoceanography 13 (1998) 491–501.
[23] S.L. Patterson, T. Whitworth, Physical oceanography, in: G.P. Glasby (Ed.), Antarctic Sector of the Pacific, Elsevier Oceanography Series, Elsevier Science Publishers, New York, 1990, pp. 55–93.
[24] A.H. Orsi, T. Whitworth III, W.D.J. Nowlin, On the meridional extent and fronts of the Antarctic Circumpolar Current, Deep-Sea Res. Part I Oceanogr. Res. Pap. 42 (1995) 641–673.
[25] K.J. Heywood, M.D. Sparrow, J. Brown, R.R. Dickson, Frontal structure and Antarctic Bottom Water flow through the Princess Elizabeth Trough, Antarctica, Deep-Sea Res. Part I Oceanogr. Res. Pap. 46 (1999) 1181–1200.
[26] L. Dezileau, G. Bareille, J.L. Reyss, F. Lemoine, Evidence for strong sediment redistribution by bottom currents along the southeast Indian ridge, Deep-Sea Res. Part I Oceanogr. Res. Pap. 47 (2000) 1899–1936.
[27] W.U. Ehrmann, H. Große, D.K. Fütterer, Late Miocene to Holocene glacial history of East Antarctica revealed by sediments from Sites 745 and 746, Proc. ODP, Scientific Results, Ocean Drilling Program 119, College Station, TX, 1991, pp. 239–251.
[28] B. Hallet, L. Hunter, J. Bogen, Rates of erosion and sediment evacuation by glaciers: a review of field data and their implications, Glob. Planet. Change 12 (1996) 213–235.
[29] R.D. Powell, Glacimarine processes and inductive lithofacies modelling of ice shelf and tidewater glacier sediments based on Quaternary examples, Mar. Geol. 57 (1984) 1–52.
[30] B.F. Molnia, Definitions and controlling factors of glacial-marine sediment and the glacial-marine sedimentary environment, Glacial-Marine Sedimentation; AGU Short Course 9, AGU, 1989, pp. 3–4.
[31] J.B. Anderson, D.S. Kennedy, M.J. Smith, E.W. Domack, Sedimentary facies associated with Antarctica's floating ice masses, in: J.B. Anderson and G.M. Ashley (Eds.), Glacial Marine Sedimentation, Paleoclimatic Significance 261, Geological Society of America, Boulder, CO, 1991, pp. 1–25.
[32] M.J. Hambrey, B. McKelvey, Neogene fjordal sedimentation on the western margin of the Lambert Graben, East Antarctica, Sedimentology 47 (2000) 577–607.
[33] W.U. Ehrmann, A. Mackensen, Sedimentological evidence for the formation of an East Antarctic ice sheet in Eocene/Oligocene time, Palaeogeogr. Palaeoclimatol. Palaeoecol. 93 (1992) 85–112.
[34] J.B. Anderson, Antarctica's glacial setting, Glacial-Marine Sedimentation, AGU Short Course 9, 1989, pp. 11–57.
[35] M.J. Hambrey, Structure and dynamics of the Lambert Glacier-Amery Ice Shelf system: implications for the origin of Prydz Bay sediments, Proc. ODP, Scientific Results, Ocean Drilling Program 119, 1991, pp. 61–75.

[36] D.K. Rea, T.R. Janecek, Mass-accumulation rates of the non-authigenic inorganic crystalline (eolian) component of deep-sea sediments from the western Mid-Pacific Mountains, Deep Sea Drilling Project Site 463, Init. Rep. DSDP 62, 1981, pp. 653–659.
[37] S.C. Clemens, W.L. Prell, Late Pleistocene variability of Arabian Sea summer monsoon winds and continental aridity: Eolian records from the lithogenic component of deep-sea sediments, Paleoceanography 5 (1990) 109–145.
[38] S.A. Hovan, Late Cenozoic atmospheric circulation intensity and climatic history recorded by eolian deposition in the eastern Equatorial Pacific Ocean, Leg 138, Proc. ODP, Scientific Results, Ocean Drilling Program 138, 1995, pp. 615–625.
[39] J.A. Barron, E. Barrera, J.-P. Caulet, B.T. Huber, B.H. Keating, D.B. Lazarus, H. Sakai, H.R. Thierstein, W. Wei, Biochronologic and magnetochronologic synthesis of Leg 119 sediments from the Kerguelen Plateau and Prydz Bay, Antarctica, Proc. ODP, Scientific Results, Ocean Drilling Program 119, 1991, pp. 813–847.
[40] S.C. Cande, D.V. Kent, Revised calibration of the geomagnetic polarity timescale for the Late Cretaceous and Cenozoic, J. Geophys. Res. 100 (1995) 6093–6095.
[41] D.K. Rea, S.A. Hovan, Grain size distribution and depositional processes of the mineral component of abyssal sediments: lessons from the North Pacific, Paleoceanography 10 (1995) 251–258.
[42] J.F. Nye, Physical Properties of Crystals, Clarendon, Oxford, 1985, 329 pp.
[43] D.H. Tarling, F. Hrouda, The Magnetic Anisotropy of Rocks, Chapman and Hall, New York, 1993, 217 pp.
[44] K.L. Boven, D.K. Rea, Partitioning of eolian and hemipelagic sediment in eastern equatorial Pacific core TR 163-31B and the late Quaternary paleoclimate of the northern Andes, J. Sediment. Res. 68 (1998) 850–855.
[45] J. Gleason, D. Rea, L. Joseph, R. Owen, J. Blum, A. Klaue, B. Klaue, Nd-Sr-Pb isotopic variations in deep-sea clays, Kerguelen Drift: a 7 my record of fluctuations in the Antarctic ice-sheet?, J. Conf. Abstr. Goldschmidt 5 (2000) 444.
[46] J.R. Breza, High resolution study of Neogene ice-rafted debris, Site 751, southern Kerguelen Plateau, Proc. ODP, Scientific Results, Ocean Drilling Program 120, 1992, pp. 207–221.
[47] S.M. Bohaty, D.M. Harwood, Southern Ocean Pliocene paleotemperature variation from high-resolution silicoflagellate biostratigraphy, Mar. Micropaleontol. 33 (1998) 241–272.
[48] J.M. Whitehead, P.F. Quilty, D.M. Harwood, A. McMinn, Early Pliocene paleoenvironment of the Sørsdal Formation, Vestfold Hills, based on diatom data, Mar. Micropaleontol. 41 (2001) 125–152.
[49] C.H. Lear, H. Elderfield, P.A. Wilson, Cenozoic deep-sea temperatures and global ice volumes from Mg/Ca in benthic foraminiferal calcite, Science 287 (2000) 269–272.
[50] S.M. Bohaty, R.P. Scherer, D.M. Harwood, Quaternary diatom biostratigraphy and palaeoenvironments of the CRP-1 Drillcore, Ross Sea, Antarctica, Terra Antarct. 5 (1998) 431–453.
[51] P.N. Webb, C.P. Strong, Recycled Pliocene foraminifera from the CRP-1 Quaternary succession, Terra Antarct. 5 (1998) 473–478.
[52] W.F. Ruddiman, A. McIntyre, Warmth of the subpolar North Atlantic Ocean during northern hemisphere ice-sheet growth, Science 204 (1979) 173–175.
[53] C. Richter, B.A. van der Pluijm, Separation of paramagnetic and ferrimagnetic susceptibilities using low temperature magnetic susceptibilities and comparison with high field methods, Phys. Earth Planet. Int. 82 (1994) 113–123.
[54] G. Denton, M. Prentice, L.H. Burckle, Cainozoic history of the Antarctic ice sheet, in: R.J. Tingey (Ed.), The Geology of Antarctica, Oxford Monographs on Geology and Geophysics 17, Clarendon Press, New York, 1991, pp. 365–432.
[55] J.B. Anderson, The Antarctic continental shelf: results from marine geological and geophysical investigations, in: R.J. Tingey (Ed.), The Geology of Antarctica, Oxford Monographs on Geology and Geophysics 17, Clarendon Press, New York, 1991, pp. 285–334.
[56] D. Weis, F.A. Frey, H. Leyrit, I. Gautier, Kerguelen Archipelago revisited: geochemical and isotopic study of the Southeast Province lavas, Earth Planet. Sci. Lett. 118 (1993) 101–119.
[57] I. Basile, F.E. Grousset, M. Revel, J.R. Petit, P.E. Biscaye, N.I. Barkov, Patagonian origin of glacial dust deposited in East Antarctica (Vostok and Dome C) during glacial stages 2, 4 and 6, Earth Planet. Sci. Lett. 146 (1997) 573–589.